FULL PAPER

ADVANCED FUNCTIONAL MATERIALS

DOI: 10.1002/adfm.200601186

α-Fe_2O_3 Nanoflakes as an Anode Material for Li-Ion Batteries

By *M. V. Reddy*, *Ting Yu*, *Chorng-Haur Sow*, *Ze Xiang Shen*, *Chwee Teck Lim*, *G. V. Subba Rao*, and *B. V. R. Chowdari**

Nanoflakes of α-Fe_2O_3 were prepared on Cu foil by using a thermal treatment method. The nanoflakes were characterized by X-ray diffraction, scanning electron microscopy, high-resolution transmission electron microscopy, and Raman spectroscopy. The reversible Li-cycling properties of the α-Fe_2O_3 nanoflakes have been evaluated by cyclic voltammery, galvanostatic discharge–charge cycling, and impedance spectral measurements on cells with Li metal as the counter and reference electrodes, at ambient temperature. Results show that Fe_2O_3 nanoflakes exhibit a stable capacity of (680 ± 20) mA h g^{-1}, corresponding to (4.05 ± 0.05) moles of Li per mole of Fe_2O_3 with no noticeable capacity fading up to 80 cycles when cycled in the voltage range 0.005–3.0 V at 65 mA g^{-1} (0.1 C rate), and with a coulombic efficiency of $>98\,\%$ during cycling (after the 15th cycle). The average discharge and charge voltages are 1.2 and 2.1 V, respectively. The observed cyclic voltammograms and impedance spectra have been analyzed and interpreted in terms of the 'conversion reaction' involving nanophase Fe^0–Li_2O. The superior performance of Fe_2O_3 nanoflakes is clearly established by a comparison of the results with those for Fe_2O_3 nanoparticles and nanotubes reported in the literature.

1. Introduction

Commercial lithium-ion batteries (LIBs) consist of $LiCoO_2$ as the positive electrode and graphite as the negative electrode.[1] To reduce the cost and improve the capacity and safety in operation, efforts are being made to find alternative electrode materials for LIBs. Nanostructured metal oxides have attracted a lot of attention in recent years as electrodes for LiBs because of their potential attributes of better chemical suitability and enlarged effective surface area.[2–9] In addition, it is possible for many of these oxides to intercalate–deintercalate Li ions into the layered (2D) or network (3D) structure.[1,3]

In recent years, nanoparticles, nanotubes, and thin films of α-Fe_2O_3 (hexagonal corundum structure) have been studied for their magnetic properties,[10] photoelectrochemical splitting of water to hydrogen,[11] photoanodic properties,[12] field-emission behavior,[13] use as potential gas sensors[14] and as electrodes for LIB applications.[14–19] Larcher et al.[16] have shown that 0.5 moles of Li can be reversibly intercalated into nanoparticles (20 nm) of α-Fe_2O_3 in the potential range 1.5–4.0 V (vs. Li). When reacted with Li to potentials up to 0.9 V (vs. Li), 2.0 moles of Li can be intercalated, but these can not be extracted electrochemically by the charging operation without destroying the crystal structure. On deep discharge with Li, up to 0.005 V (vs. Li), as many as 8.5 moles of Li per mole of Fe_2O_3 react, with the concomitant crystal structure destruction and formation of nanometer-sized metal particles (Fe^0), Li_2O, and a polymeric layer on Fe^0 as a result of the decomposition of the solvents in the electrolyte.[16] The subsequent charging operation, up to 3.0 V (vs. Li), can result in the release of Li ions (and electrons) by the 'conversion reaction' of nanometer-sized Fe^0 particles with Li_2O.[1–3] Studies by Larcher et al.[18] and Morales et al.[17] on α-Fe_2O_3 nanoparticles and by Chen et al.[14] on α-Fe_2O_3 nanotubes have clearly indicated that the morphology of nanometer-sized α-Fe_2O_3 structures plays a significant role in the reactivity of the material towards Li, and have shown that 4 moles of Li are cyclable in the potential range 0.005–3.0 V, but capacity degradation occurred in all cases on long-term cycling.

Recently we developed a simple thermal treatment (hotplate) technique for the realization of nanowalls and nanoflakes of metal oxides on suitable substrates.[13,20,21] In this Full Paper, we report on the preparation and electrochemical performance of nanoflakes of α-Fe_2O_3 films on a Cu substrate, examined by using cyclic voltammetry, charge–discharge cycling, and impedance spectral analysis. Results show that 4.0 moles of Li are cyclable up to 80 cycles without any capacity degradation, thereby establishing the advantage of nanoflake morphology over the nanoparticle/nanotube morphology of α-Fe_2O_3 for reversible Li storage.

[*] Prof. B. V. R. Chowdari, Dr. M. V. Reddy, Prof. C. H. Sow, Prof. G. V. Subba Rao
Department of Physics
National University of Singapore
Singapore 117542 (Singapore)
E-mail: phychowd@nus.edu.sg
Dr. Ting Yu, Prof. Z. X. Shen
Division of Physics and Applied Physics
Nanyang Technological University
Singapore 637616 (Singapore)
Prof. C. T. Lim
Department of Mechanical Engineering
National University of Singapore
Singapore 117576 (Singapore)

2. Results and Discussion

2.1. Characterization

In a previous publication,[13] we described the formation of nanoflakes of α-Fe_2O_3 on various substrates by the thermal heating method, and we also suggested a plausible mechanism for the growth of nanoflakes. Briefly, the nature and density of the nanoflakes depends on the nature of the (Cu, Fe metal, or Si) substrate, thickness of the deposited Fe film, the temperature and time of heating of the foil in an air/oxygen/inert atmosphere. Presently, we employed an etched copper foil as substrate, an Fe film of thickness of approximately 700 nm, a temperature of 300 °C, and a 5 h heating time in air to obtain adherent and dense flakes of α-Fe_2O_3. Figure 1 shows a field-emission scanning electron microscopy (FE-SEM) image of the Fe_2O_3 nanoflakes obtained on the Cu substrate. The nanometer-sized flakes are generally pointed perpendicular to the plane of the Cu substrate. Naturally, these nanoflakes present a large effective area, which would be potentially significant for electrochemical performance. Figure 2a shows the typical transmission electron microscopy (TEM) image of the α-Fe_2O_3 nanoflakes, and Figure 2b shows the high-resolution TEM (HR-TEM) lattice image. The measured lattice spacing of 0.371 nm is in good agreement with the *d*-spacing of the (012) plane (0.368 nm) of α-Fe_2O_3.[13] Raman spectroscopy (Fig. 3) further supports the presence of α-Fe_2O_3 together with a small amount of Fe_3O_4, which is believed to be the precursor for the growth of the Fe_2O_3 nanoflakes.[13] The X-ray diffraction (XRD) pattern of the nanoflakes (not shown) indicated the phase to be α-Fe_2O_3 along with some Fe_3O_4.[13]

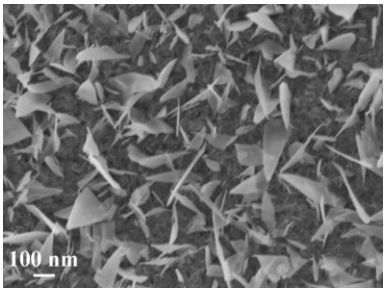

Figure 1. Field-emission scanning electron microscopy image of α-Fe_2O_3 nanoflakes grown on a Cu substrate. Scale bar: 100 nm.

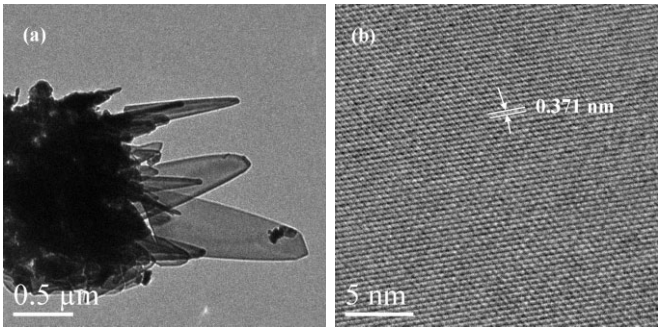

Figure 2. High-resolution transmission electron microscopy images of α-Fe_2O_3 a) nanoflakes, and the corresponding b) lattice image. The interplanar spacing is 0.371 nm.

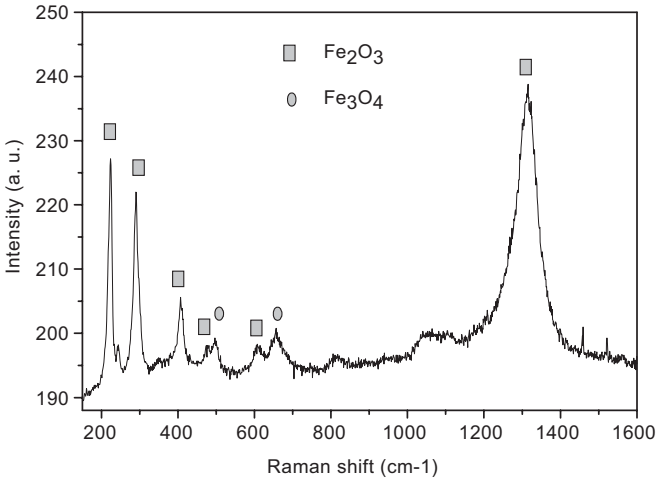

Figure 3. Raman spectrum of α-Fe_2O_3 nanoflakes. The bands due to Fe_3O_4 impurity are also indicated.

2.2. Electrochemical Studies

2.2.1. Galvanostatic Cycling

Discharge–charge cycling was carried out in the voltage window of 0.005–3.0 V (vs. Li) at a current density of 65 mA g^{-1} up to 80 cycles at ambient temperature (RT), and the voltage versus capacity profiles are shown in Figure 4. For clarity, only selected cycles are shown. The open-circuit voltage (OCV) of the fabricated and aged (12 h) cells was about 3.0 V. During the first discharge, the voltage decreased steeply to approximately 1.2 V, whereupon a plateau sets in and continues until a capacity of about 300 mA h g^{-1} is reached. This corresponds to a consumption of 1.8 moles of Li per mole of Fe_2O_3. Another voltage plateau is observed at about 0.75 V up to a capacity of approximately 800 mA h g^{-1}, followed by a gradual drop in voltage until the end of discharge. The total first-discharge capacity is (1235 ± 20) mA h g^{-1} and corresponds to a consumption of 7.4 moles of Li per mole of Fe_2O_3. The plateaux voltages are clearly reflected as peaks in the differential capacity versus voltage plots shown in Figure 4b and c. These peaks indicate a two-phase reaction, due to the coexistence of two phases. The first-discharge profile qualitatively resembles that noted by Larcher et al.[18] and Morales et al.[17] on nanoparticulate Fe_2O_3 and Chen et al.[14] on nanotubes of Fe_2O_3. However, our plateaux voltage values are smaller, and the total first-discharge capacity is also smaller, 7.4 moles of Li versus 8.8 observed by Larcher et al.[18] and Chen et al.,[14] and 8.3 moles of Li reported by Morales et al.[17] These facts indicate that the morphology of the nanostructured Fe_2O_3 plays a significant role in determining the discharge characteristics.

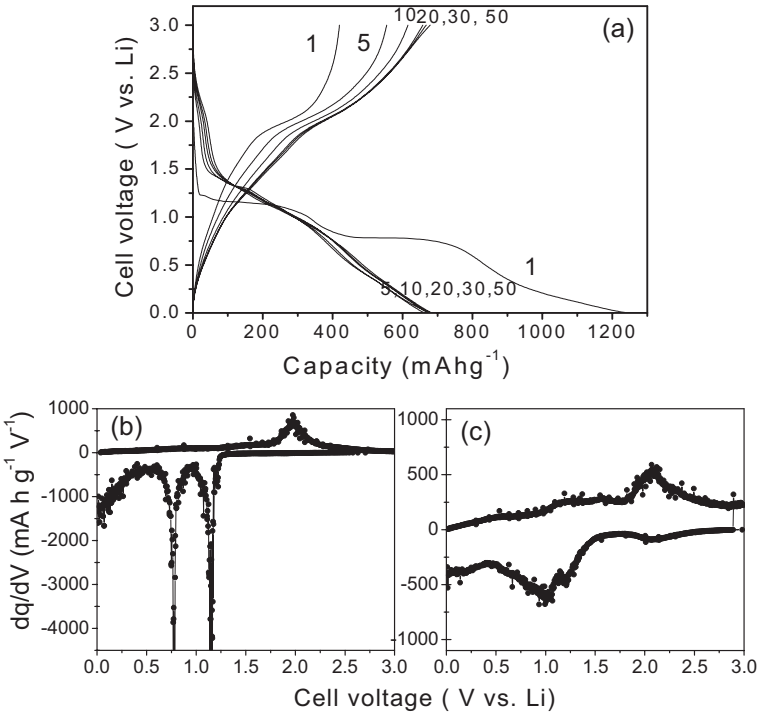

Figure 4. a) Galvanostatic charge–discharge curves of α-Fe_2O_3 nanoflakes in the voltage range 0.005–3.0 V (vs. Li) at a current of 65 mA g^{-1}. The numbers indicate cycle number. b) The 1st cycle, and c) 50th cycle differential capacity, dq/dV [mA h g^{-1} V^{-1}], versus voltage ([V] vs. Li) plots extracted from (a).

According to the reaction mechanism proposed in the earlier studies,[14,16–18] the first voltage plateau at approximately 1.2 V (and consumption of 1.8 moles of Li) in the nanostructured Fe_2O_3 represents the coexistence of two Li-intercalated phases, hexagonal and cubic, as per Equation 1:

$$Fe_2O_3 + 2\,Li^+ + 2\,e^- \rightarrow Li_2(Fe_2O_3) \quad (1)$$

$$Li_2(Fe_2O_3) + 4\,Li^+ + 4\,e^- \rightarrow 2\,Fe^0 + 3\,Li_2O \quad (2)$$

$$2\,Fe^0 + 2\,Li_2O \leftrightarrow 2\,Fe^{II}O + 4\,Li^+ + 4\,e^- \quad (3)$$

The second voltage plateau, at about 0.75 V, represents the reduction of Fe ions to form nanometer-sized Fe metal (Fe^0) and amorphous Li_2O, preceded by crystal structure destruction, given by Equation 2. The additional consumption of 1.4 moles of Li is presently observed, over and above those given in Equations 1 and 2, below 0.75 V, caused by the formation of a solid electrolyte interphase (SEI) and the polymeric gel-type layer on the metal nanoparticles because of the decomposition of the solvent in the electrolyte. The first-charge reaction is represented by the forward reaction of Equation 3, where the decomposition of Li_2O is aided by the nanostructured Fe^0, resulting in the formation of FeO and giving a capacity corresponding to 4 moles of Li. The subsequent reversible discharge–charge reactions follow Equation 3.

The first-charge profile of the Fe_2O_3 nanoflakes shows a strong polarization near 1.4 V followed by a voltage plateau at about 2.0 V, suggesting two-phase coexistence (Fig. 4a and b). The first-charge capacity is 420 mA h g^{-1} (ca. 2.6 moles of Li), which is smaller than the expected theoretical value of 671 mA h g^{-1} (4.0 moles of Li) as per Equation 3. The discharge–charge profiles shown in the 5–50 cycles range in Figure 4a indicate that, while the discharge curves overlap reasonably well, the charge curves shift towards increasing capacity and merge during the 20th–50th cycles. This shows that full and stable capacity is realized only after 15–20 cycles, possibly due to the nature of the Fe_2O_3 nanoflakes. The exact reason for this 'conditioning' or 'formation' of the electrode extending up to the initial 15th cycle is not clear at present. As no conducting carbon was employed for the fabrication of the electrode of α-Fe_2O_3 nanoflakes, it is obvious that the 'nanostructured Fe^0–amorphous Li_2O' composite formed during the first discharge reaction (Eq. 2) needs several charge–discharge cycles for stable SEI film formation, percolation of the electrolyte through all the nanoflakes of the electrode, and to establish intimate electrical (electronic) contact with the Cu current collector. We note that an increase in the reversible capacity with cycle number was observed earlier by Guyomard et al.[22] in the Li_xMVO_4 (M=metal) system, and recently by Yu et al.[23] in the Ni-foam-supported reticular 'CoO–Li_2O' thin-film composite anode, and by Taberna et al.[8] in the Cu-nanopillar-supported Fe_3O_4 anode. In the latter two of the above systems, the electrodes did not contain any conducting carbon or additive, as is the case in the present study. Thus, it appears that whenever conducting carbon is not employed for the fabrication, 'formation' of the electrode can extend to several cycles for the full realization of the inherent reversible capacity.

The differential capacity versus voltage plot for the 50th cycle, shown in Figure 4c, indicates that the average discharge voltage is about 1.2–1.3 V and the charge voltage is 2.1 V. The capacity versus cycle number plot is shown in Figure 5. As can be seen, the discharge capacity decreases while the charge capacity increases up to 15 cycles, and thereafter stabilizes to give almost identical values up to 80 cycles, with no noticeable capacity fading. The stable and reversible capacity of (680 ± 20) mA h g^{-1} corresponds to (4.0 ± 0.05) moles of Li per mole of Fe_2O_3, which is in excellent agreement with Equation 3. It is also clear from Figures 4a and 5 that the Coulombic efficiency is > 98 % in the 20–80 cycles range, at a current of 65 mA g^{-1}, which corresponds to about the 0.1 C rate (1 C = 680 mA g^{-1}). A comparison of the cycling performance of Fe_2O_3 nanoflakes with those of Fe_2O_3 nanoparticles[17] and Fe_2O_3 nanotubes[14] shows that the latter two phases, cycled at 0.2 C and 0.07 C rates, respectively, showed fairly large capacity fading: Thus, only 56 and 54 % of the initial capacity was retained at the end of 15 and 100 cycles, respectively, in the case of Fe_2O_3 nanoparticles and Fe_2O_3 nanotubes. Hence, the nano-

ADVANCED FUNCTIONAL MATERIALS

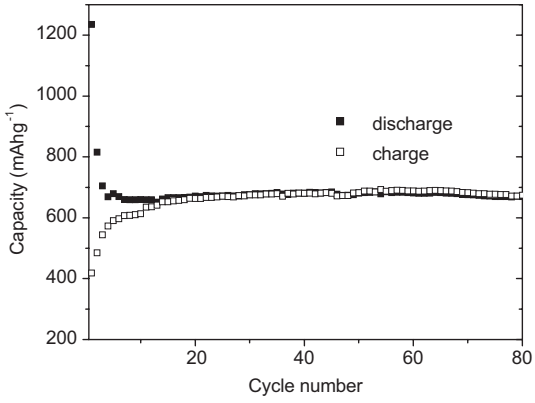

Figure 5. Capacity versus cycle number plot of α-Fe_2O_3 nanoflakes, cycled in the voltage range of 0.005–3.0 V at a current of 65 mA g^{-1} (0.1 C rate). Filled and open symbols represent discharge and charge capacity, respectively.

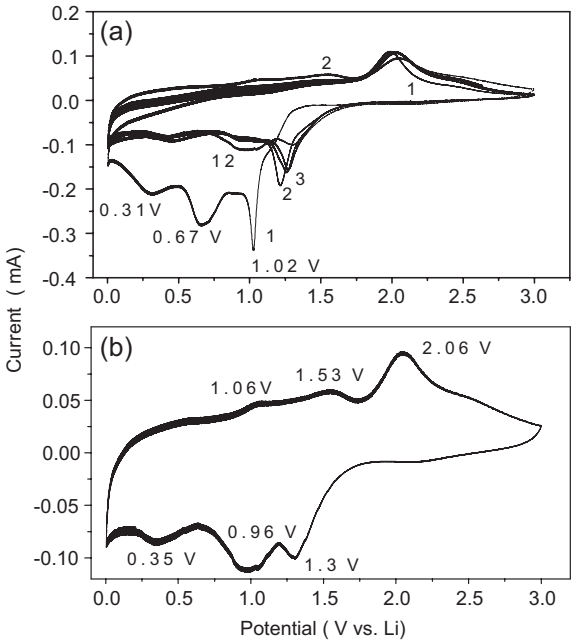

Figure 6. a) Cyclic voltammograms of α-Fe_2O_3 nanoflakes. Voltage range, 0.005–3.0 V; scan rate, 58 μV s^{-1}. Numbers represent the cycle number. Peak potentials are also shown. b) Cyclic voltammogram of the 12th cycle on an expanded scale. Peak potentials are shown. Li metal was used for both the reference and counter electrodes.

flake nature of the starting Fe_2O_3 with defect-free flakes, good adhesion of the flakes with each other and to the current collector, and maintenance of integrity in spite of the structure destruction/reduction during the processes of Equations 1 and 2, and renewal of particle surfaces during the reactions of Equation 3 seem to act in a favorable manner to give rise to the observed stable and large reversible capacities.

2.2.2. Cyclic Voltammetry (CV)

Cyclic voltammograms were recorded on the cells with α-Fe_2O_3 nanoflakes at ambient temperature (RT) in the 0.005–3.0 V range at a slow scan rate of 58 μV s^{-1} up to 15 cycles. Li metal was used as the counter and reference electrodes. These results are shown in Figure 6. Only selected cycles are shown for clarity. The first sweep was cathodic (reaction with Li) and started from the OCV (ca. 2.9 V). As can be seen, a smooth sloping curve up to about 1.02 V with a shoulder at about 1.2 V is indicative of the single-phase insertion of Li and reduction of Fe^{3+} ions in α-Fe_2O_3, and the coexistence of two intercalated phases, as described earlier (Fig. 4a and b). This is followed by the onset of a peak at about 0.8 V. Well-defined peaks are observed at 0.67 V and 0.31 V. These peaks are also reflected in the differential capacity plots of Figure 4b. These correspond to Equation 2 and probably occur in two steps. The subsequent charge (anodic) curve is smooth up to 1.75 V and shows a peak at about 2.04 V, which nearly coincides with the voltage plateau in the galvanostatic charging curve (Fig. 4a and b).

The second cathodic sweep differs from the first one, indicating a different mechanism: a sharp cathodic peak at approximately 1.2 V and broad peaks at about 0.96 and 0.35 V are seen. The peak at 0.67 V, noticed in the first cathodic scan, is now absent. In the second anodic scan (Li removal), indication of small peaks at about 1.0 and 1.5 V are seen, in addition to the main peak at 2.1 V. During the 3rd–12th cycles, the CV peaks overlap well, indicating good reversibility of the discharge–charge reactions. The CV result for the 12th cycle, showing the well-defined cathodic and anodic peaks, bears very good resemblance to the 50th cycle differential capacity versus potential plot of Figure 4c, indicating the complementary nature of the galvanostatic and CV data.

Chen et al.[14] reported CV results of Fe_2O_3 nanotubes up to 20 cycles recorded at a high scan rate of 0.5 mV s^{-1}. Morales et al.[17] also reported step-potential curves up to 5 cycles, which are equivalent cyclic voltammograms, on Fe_2O_3 nanoparticles. A comparison of the these results with our CV data indicate that qualitatively the curves are similar. However, while the anodic peak potential value of around 2.1 V observed by Chen et al.[14] agrees well with our value, those of the cathodic peaks differ nontrivially, possibly because of the nanotube nature of their starting material and the high scan rate employed by them. Similarly, minor differences exist between our CV curves and those of Morales et al.,[17] reflecting the differences in behavior between the nanoparticles and nanoflakes of Fe_2O_3.We must mention here that the observation of multiple peaks in the CV results, complemented by the differential capacity versus potential curves (Figs. 6b and 4c), indicates that the reversible reactions of Equation 3 occur not as a single well-defined step but via two or more steps that involve intermediate coexisting phases. It is also possible that during the charging process, oxidation may occur not only from Fe^0 to Fe^{2+}, but also partly from Fe^{2+} to Fe^{3+}, as indeed noticed by Morales et al.[17] by ex situ X-ray photoelectron spectroscopy measurements.

2.2.3. Electrochemical Impedance Spectroscopy

Impedance spectral measurements on electrode materials can give important information regarding the factors responsible for Li cycling, like the surface film and charge-transfer resistances, the associated capacitances and their variation with the applied voltage, including the fully discharged and fully charged states. Thus, impedance data on several oxide cathodes like $Li_{1-x}CoO_2$,[24] $Li_{1-x}(Ni_{1/3}Mn_{1/3}Co_{1/3})O_2$,[25] and anodes like Li_x–graphite[26] have been analyzed and interpreted, in which single-phase (solid-solution) reactions occur for a limited range of x. However, impedance studies have also been reported on oxide anodes like SnO,[27] $K_2(Li_{2/3}Sn_{22/3})O_{16}$,[28] Co_3O_4,[29,30] $Ca_2Co_2O_5$,[31] $TiOF_2$ and NbO_2F,[32] $Li_4Ti_5O_{12}$,[33] and the 3.5 V cathode, $LiFePO_4$.[34–36] In the above systems, either 'alloying–de-alloying', or 'conversion', or 'deintercalation–intercalation' reactions occur with Li, essentially in the form of two-phase reactions, and, strictly speaking, the derived impedance parameters may not be of any significance. However, the relative variations in the impedance parameters, namely, surface-film and charge-transfer resistances, surface-film and double-layer capacitances, and so on, at various values of x (at various voltages) do have a significance and represent the changes taking place in the systems, and possibly reveal the reaction mechanisms. No impedance data are available in the literature on nanoparticles or nanotubes of Fe_2O_3.

Here, impedance measurements were carried out at room temperature on cells with Fe_2O_3 nanoflakes versus Li at selected voltages in the range of 0.005–3.0 V at a slow scan rate of 58 $\mu V s^{-1}$ during the first discharge–charge cycle and also during the 42nd cycle. The cells were discharged or charged to a particular voltage value and relaxed for 1 h and the impedance was measured. The Nyquist plots (Z' versus $-Z''$) at various voltage values during the 1st discharge cycle are shown Figure 7a. The impedance data were analyzed by fitting to an equivalent electrical circuit shown in Figure 7c, similar to the circuit employed for other oxide electrodes.[28,32,34,35] It consists of the electrolyte (R_e), surface film (R_{sf}), and charge transfer (R_{ct}) resistances, a constant phase element (CPE_i) instead of pure capacitance (due to the observation of a depressed semicircle), along with suitable diffusional components like Warburg impedance (W_s) and the intercalation capacitance (C_{int}). The impedance of CPE is defined as $Z_{CPE} = 1/[B(j\omega)^{\alpha}]$ where $j = \sqrt{-1}$, ω is the angular frequency, and B and α are constants. The value of α gives the degree of distortion of the impedance spectra and when $\alpha = 1$, B is identical to C_i and CPE_i becomes an ideal capacitor. The resistance R_{ct} arises due to Li-ion charge-transfer resistance at the interface between the electrode and electrolyte, whereas R_{sf} refers to the surface-film resistance.

In Figures 7 and 8, the symbols are the experimental data whereas the continuous lines represent the fitted spectra. The derived parameters including α are given in Table 1. The fresh cell (OCV of ca. 3.0 V) shows a single broad depressed semicircle in the high-frequency region (>1 kHz), which reveals, after curve fitting, an impedance of (266±5) Ω, attributed mainly to R_{sf}. The associated capacitance (CPE_{sf}) is (33±5) μF. The spectrum measured at the voltage of 1.5 V differs markedly from the initial one recorded at the OCV (Fig. 7a). The diameter of the semicircle reduces drastically followed by the well-defined Warburg region at low frequencies. This shows that R_{sf} is reduced drastically and R_{ct} comes in to prominence because of the initiation of the intercalation/decomposition reaction of Li into nanoflakes of Fe_2O_3. However, due to the observed single semicircle, the curve fitting was carried out using $R_{(sf+ct)}$ combination. This value is (48±5) Ω and the corresponding $CPE_{(sf+dl)}$ (dl=double layer) is (18±5) μF. The spectra measured in the voltage range 0.9–0.2 V are qualitatively similar,

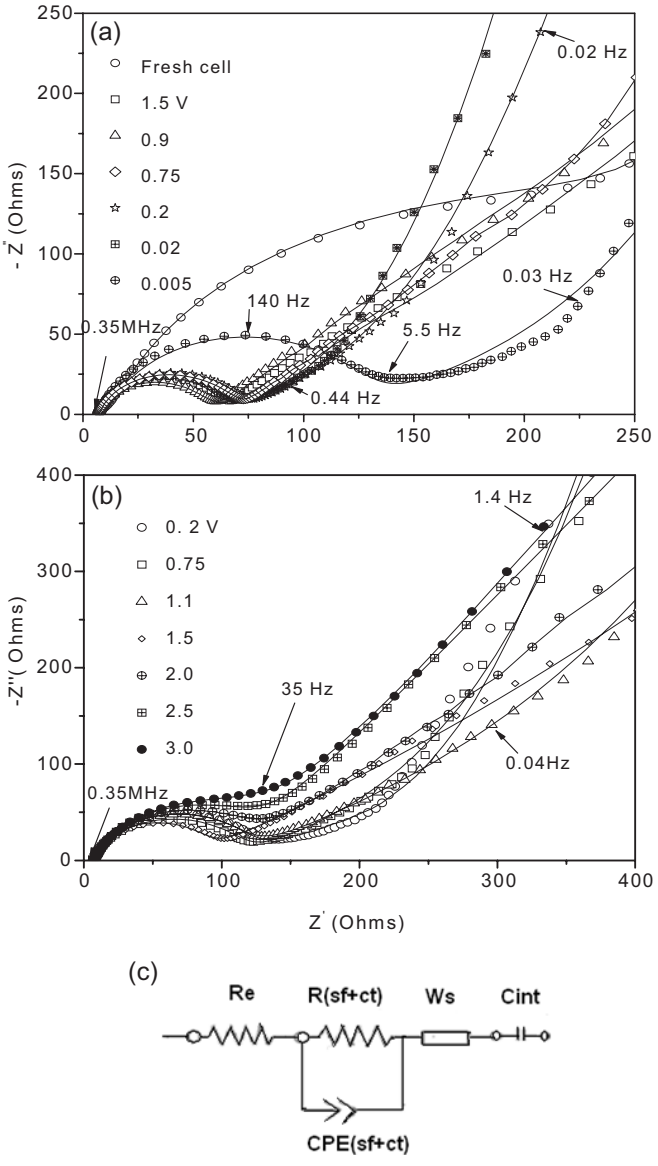

Figure 7. Nyquist plots (Z' vs. $-Z''$) of α-Fe_2O_3 nanoflakes, during the first cycle, at various voltages. a) Discharge cycle. b) Charge cycle. Symbols represent experimental spectra and continuous lines represent fitted data using the equivalent electrical circuit shown in (c). See text for explanation of variables shown in circuit. Voltage range, 0.005–3.0 V (vs. Li). The voltage values and selected frequencies are shown. Geometrical area of the electrode is 2.0 cm × 2.0 cm.

ADVANCED FUNCTIONAL MATERIALS

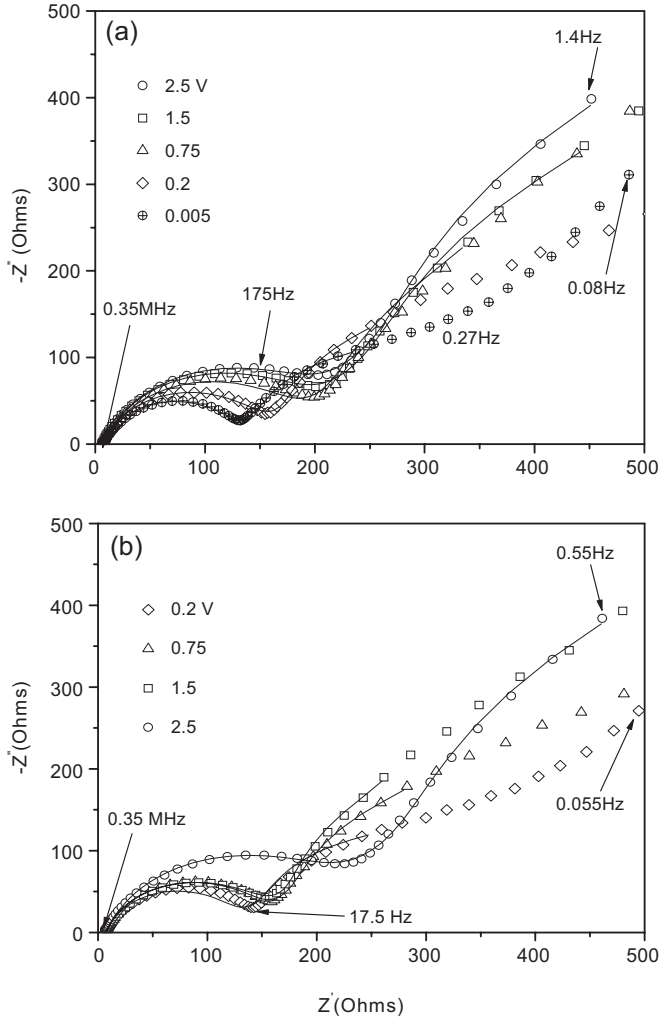

Figure 8. Nyquist plots (Z' vs. $-Z''$) of α-Fe_2O_3 nanoflakes during the 42nd cycle. a) Discharge cycle. b) Charge cycle. Symbols represent experimental spectra and continuous lines represent fitted data using the equivalent electrical circuit of Figure 7c. Voltage range: 0.005–3.0 V (vs. Li). The voltage values and selected frequencies are shown. Geometrical area of the electrode is 2.0 cm × 2.0 cm.

with $R_{(sf+ct)}$ values lying in the range (47 ± 5–53 ± 5) Ω (Table 1). On the other hand, the spectrum recorded at 0.005 V, the deep discharge limit, shows a large-diameter semicircle and the fitted value of $R_{(sf+ct)}$ is (108 ± 5) Ω, which is almost twice the value obtained at 0.2 V. The $CPE_{(sf+dl)}$ values remain in the range (22 ± 5–30 ± 5) μF for the applied voltages of 0.9–0.005 V. The extracted values of α are between 0.81–0.91 during the first discharge, and indicate the nonideal nature of the electrode because of porosity and the nonuniform charge-transfer properties of the oxide electrode.[24,32,37]

The impedance spectra during the first charge cycle are qualitatively similar and are shown in Figure 7b. The calculated values of $R_{(sf+ct)}$ and $CPE_{(sf+dl)}$ go through a minimum of (71 ± 5) Ω, and (14 ± 5) μF, respectively, whereas α goes through a maximum (0.94) at 1.5 V (Table 1).

Figure 8 shows the impedance spectra of Fe_2O_3 nanoflakes at selected voltages during the 42nd discharge–charge cycle, and the derived parameters are given in Table 1. The spectra during the discharge cycle as well as charge cycle are qualitatively similar, indicating good reversibility of the electrode. As can be seen from Table 1, the $R_{(sf+ct)}$ value monotonically decreases during the 42nd discharge cycle from (170 ± 5) to (112 ± 5) Ω, and increases during the corresponding charge cycle from (119 ± 5 to (199 ± 5) Ω (Table 1) in the voltage range 0.005 to 2.5 V. The corresponding $CPE_{(sf+dl)}$ values are in the range (13 ± 5–19 ± 5) μF and do not show any systematic variation. Similarly, the α values are almost constant at (0.84 ± 0.02). Thus, the impedance data corroborate the galvanostatic cycling data. The resistance value of the electrolyte and cell components (R_e) was (5 ± 1) Ω, and the intercalation capacitance C_{int} was in the range 0.15–5.0 (± 0.1) F at all voltages during the first and 42nd discharge–charge cycles. These values are reasonable and are encountered in studies on other oxide anode and cathode materials.[24,32,36,38]

3. Conclusions

We prepared Fe_2O_3 nanoflakes on copper substrates by a simple hotplate technique and characterized the material by XRD, SEM, HR-TEM, and Raman spectroscopy techniques. The electrochemical Li-cycling behavior of the nanoflakes has been tested by galvanostatic discharge–charge cycling, CV, and impedance methods. Results show that the α-Fe_2O_3 nanoflakes exhibit stable capacity of (680 ± 20) mA h g^{-1}, with no noticeable capacity fading up to 80 cycles, when cycled in the range of 0.005–3.0 V at 65 mA g^{-1} (0.1 C rate). This value corresponds to the theoretical capacity of (4.05 ± 0.05) moles of Li, as per Equation 3. A coulombic efficiency (η) of > 98 % is shown after the 15th cycle. The average discharge and charge voltage values are 1.2 and 2.1 V, respectively. Impedance studies were carried out at various voltages during the 1st discharge–charge cycle and the 42nd cycle, and the derived impedance parameters were interpreted. The performance of the α-Fe_2O_3 nanoflake material has been compared with the reported data on nanoparticle Fe_2O_3 and nanotube Fe_2O_3, which both showed capacity fading on cycling. In a very recent report, the group of Yamaki[39] also observed drastic capacity fading after 20 cycles with nanoparticles of Fe_2O_3 loaded with acetylene black. These results, combined with the fact that iron oxides are cheap, abundant, and environmentally compatible, make the Fe_2O_3 nanoflakes an alternative anode material to replace the presently used graphite in LIBs.

4. Experimental

Preparation: A thin Fe film was deposited on Cu foil (16 mm in diameter and 50 μm thick circular disks; purity, 99 %) by using radio frequency (rf) magnetron sputtering (Denton Vacuum Discovery 18 system). The deposition conditions used were: rf power, 150 W; total pressure, 10 mtorr (1 torr = 133.3 Pa); deposition time, 90 min; substrate temperature, 25 °C. Several films were prepared with a thickness of about 700 nm. Subsequently, the Fe-coated Cu foils were heated on a hotplate at 300 °C for 5 h in air to form the nanoflakes. Details of the

Table 1. Impedance parameters of the cell, with α-Fe_2O_3 nanoflakes as the cathode and a Li-metal anode, during the 1st and 42nd discharge–charge cycles at various voltages.

Parameter values							
				First discharge cycle			
Cell voltage [V]	3.0	1.5	0.9	0.75	0.2	0.02	0.005
$R_{(sf+ct)}$ (±5) [Ω]	266	48	47	55	58	53	108
$CPE_{(sf+dl)}$ (±5) [μF]	33	18	30	22	24	26	26
α (±0.02) [a]	0.81	0.91	0.84	0.88	0.87	0.86	0.85
				First charge cycle			
Cell voltage [V]	0.2	0.75	1.1	1.5	2.0	2.5	3.0
$R_{(sf+ct)}$ (±5) [Ω]	104	99	98	71	106	104	117
$CPE_{(sf+dl)}$ (±5) [μF]	24	29	20	14	27	21	37
α (±0.02) [a]	0.86	0.83	0.89	0.94	0.85	0.88	0.81
				42^{nd} discharge cycle			
Cell voltage [V]	2.5	1.5	0.75	0.2	0.005		
$R_{(sf+ct)}$ (±5) [Ω]	170	169	164	140	112		
$CPE_{(sf+dl)}$ (±5) [μF]	13	14	17	17	17		
(α (±0.02) [a]	0.85	0.85	0.83	0.84	0.85		
				42nd charge cycle			
Cell voltage [V]	0.2	0.75	1.5	2.5			
$R_{(sf+ct)}$ (±5) [Ω]	119	137	144	199			
$CPE_{(sf+dl)}$ (±5) [μF]	19	18	18	13			
α (±0.02) [a]	0.83	0.82	0.86	0.85			

[a] Evaluated from the equation, $Z_{CPE} = 1/[B(j\omega)^{\alpha}]$.

preparation of α-Fe_2O_3 nanoflakes on a wide variety of substrates have been described elsewhere [13].

Characterization: The α-Fe_2O_3 nanoflakes were characterized by field-emission scanning electron microscopy (FE-SEM; JEOL GSM 6700F) and high-resolution TEM (HR-TEM, JEOL JEM-2010F, 200 kV) for morphology and lattice images. Micro-Raman spectroscopy (ISA T640000 Triple grating system, Ar laser, $\lambda = 514.5$ nm) and X-ray diffraction (D8 Bruker) were employed for phase identification.

Electrochemical Measurements: The working electrode consisted of nanoflakes of α-Fe_2O_3 on Cu foil used as the current collector (thickness ca. 700 nm). We note that no conducting carbon or binder was used for the fabrication of the above thin-film electrode. The geometrical area of the electrode was 2.0 cm × 2.0 cm and the amount of active material was ca. 0.7 mg. Coin-type test cells (size 2016) were assembled by using an electrode consisting of α-Fe_2O_3 nanoflakes, Li-metal foil (0.59 mm thick; Kyokuto Metal Co., Japan) as both the counter (anode) and reference electrodes, 1 M solution of $LiPF_6$ in ethylene carbonate (EC) and diethyl carbonate (DEC) (1:1 by volume; Merck) as the electrolyte, and polypropylene foil (Celgard) as the separator. The cells were fabricated in an argon-filled glove box (M. Braun, Germany). Other details of cell fabrication have been described elsewhere [28,32,38,40]. The cells were aged for 12 h before measurement. The cyclic voltammetry and charge–discharge cycling were carried out at ambient temperature (RT = 24 °C) by using a Macpile II system (Biologic, France) and multichannel battery tester (model SCN, Bitrode, USA), respectively. Electrochemical impedance measurements were carried out with a Solartron impedance/phase-gain analyzer (model SI 1255) coupled with a battery test unit (model 1470). The frequency range was from 0.35 MHz to 3 mHz with an ac signal amplitude of 5 mV. Data were analyzed using *Z*-plot and *Z*-view software (Version 2.2, Scribner Associates, USA) to obtain the Nyquist plots.

Received: December 12, 2006
Revised: May 3, 2007
Published online: August 17, 2007

[1] *Lithium Batteries: Science and Technology* (Eds: G.-A. Nazri, G. Pistoia), Kluwer Academic, New York **2003**.
[2] P. Poizot, S. Laruelle, S. Grugeon, L. Dupont, J.-M. Tarascon, *Nature* **2000**, *407*, 496.
[3] A. S. Arico, P. G. Bruce, B. Scrosati, J.-M. Tarascon, W. V. Schalkwijk, *Nat. Mater.* **2005**, *4*, 366.
[4] N. Li, C. R. Martin, B. Scrosati, *Electrochem. Solid-State Lett.* **2000**, *3*, 316.
[5] V. Subramanian, J. C. Jiang, P. H. Smith, B. Rambabu, *J. Nanosci. Nanotechnol.* **2004**, *4*, 125.
[6] S. Grugeon, S. Laruelle, L. Dupont, F. Chevallier, P. L. Taberna, P. Simon, L. Gireaud, S. Lascaud, E. Vidal, B. Yrieix, J.-M. Tarascon, *Chem. Mater.* **2005**, *17*, 5041.
[7] X. Li, F. Cheng, B. Guo, J. Chen, *J. Phys. Chem. B* **2005**, *109*, 14 017.
[8] P. L. Taberna, S. Mitra, P. Poizot, P. Simon, J.-M. Tarascon, *Nat. Mater.* **2006**, *5*, 567.
[9] M. V. Reddy, B. Pecquenard, P. Vinatier, A. Levasseur, *J. Phys. Chem. B* **2006**, *110*, 4301.
[10] L. Lu, H.-Z. Kou, W. Mo, H. Liu, Y. Wang, *J. Phys. Chem. B* **2006**, *110*, 15 218.
[11] S. U. M. Khan, J. Akikusa, *J. Phys. Chem. B* **1999**, *103*, 7184.
[12] A. Watanabe, H. Kozuka, *J. Phys. Chem. B* **2003**, *107*, 12 713.
[13] T. Yu, Y. W. Zhu, X. J. Xu, K. S. Yeong, Z. X. Shen, P. Chen, C. T. Lim, J. T. L. Thong, C. H. Sow, *Small* **2006**, *2*, 80.
[14] J. Chen, L. Xu, W. Li, X. Gou, *Adv. Mater.* **2005**, *17*, 582.
[15] J. Sarradin, A. Guessous, M. Ribes, *J. Power Sources* **1996**, *62*, 149.
[16] D. Larcher, C. Masquelier, D. Bonnin, Y. Chabre, V. Masson, J.-B. Leriche, J.-M. Tarascon, *J. Electrochem. Soc.* **2003**, *150*, A133.
[17] J. Morales, L. Sánchez, F. Martín, F. Berry, X. Ren, *J. Electrochem. Soc.* **2005**, *152*, A1748.
[18] D. Larcher, D. Bonnin, I. Rivals, L. Personnaz, J.-M. Tarascon, *J. Electrochem. Soc.* **2003**, *150*, A1643.

[19] G. Jain, M. Balasubramanian, J. J. Xu, *Chem. Mater.* **2006**, *18*, 423.
[20] T. Yu, X. Zhao, Z. Shen, Y. Wu, W. Su, *J. Cryst. Growth* **2004**, *268*, 590.
[21] T. Yu, Y. Zhu, X. Xu, Z. Shen, P. Chen, C.-T. Lim, J. T. L. Thong, C. H. Sow, *Adv. Mater.* **2005**, *17*, 1595.
[22] D. Guyomard, C. Sigala, A. Le Gal La Salle, Y. Piffard, *J. Power Sources* **1997**, *68*, 692.
[23] Y. Yu, C.-H. Chen, J.-L. Shui, S. Xie, *Angew. Chem. Int. Ed.* **2005**, *44*, 7085.
[24] F. Nobili, R. Tossici, R. Marassi, F. Croce, B. Scrosati, *J. Phys. Chem. B* **2002**, *106*, 3909.
[25] K. M. Shaju, G. V. Subba Rao, B. V. R. Chowdari, *J. Electrochem. Soc.* **2004**, *151*, A1324.
[26] M. D. Levi, D. Aurbach, *J. Phys. Chem. B* **1997**, *101*, 4630.
[27] D. Aurbach, A. Nimberger, B. Markovsky, E. Levi, E. Sominski, A. Gedanken, *Chem. Mater.* **2002**, *14*, 4155.
[28] N. Sharma, J. Plévert, G. V. Subba Rao, B. V. R. Chowdari, T. J. White, *Chem. Mater.* **2005**, *17*, 4700.
[29] Y.-M. Kang, M.-S. Song, J.-H. Kim, H.-S. Kim, M.-S. Park, J.-Y. Lee, H. K. Liu, S. X. Dou, *Electrochim. Acta* **2005**, *50*, 3667.
[30] S. A. Needham, G. X. Wang, K. Konstantinov, Y. Tournayre, Z. Lao, H. K. Liu, *Electrochem. Solid-State Lett.* **2006**, *9*, A315.
[31] N. Sharma, K. M. Shaju, G. V. Subba Rao, B. V. R. Chowdari, *Electrochim. Acta* **2004**, *49*, 1035.
[32] M. V. Reddy, S. Madhavi, G. V. Subba Rao, B. V. R. Chowdari, *J. Power Sources* **2006**, *162*, 1312.
[33] G. X. Wang, D. H. Bradhurst, S. X. Dou, H. K. Liu, *J. Power Sources* **1999**, *83*, 156.
[34] G. X. Wang, L. Yang, Y. Chen, J. Z. Wang, S. Bewlay, H. K. Liu, *Electrochim. Acta* **2006**, *51*, 4634.
[35] H. C. Shin, W. I. Cho, H. Jang, *J. Power Sources* **2006**, *159*, 1383.
[36] M. Koltypin, D. Aurbach, L. Nazar, B. Ellis, *Electrochem. Solid-State Lett.* **2007**, *10*, A40.
[37] M. D. Levi, D. Aurbach, *J. Phys. Chem. B* **2004**, *108*, 11 693.
[38] K. S. Tan, M. V. Reddy, G. V. Subba Rao, B. V. R. Chowdari, *J. Power Sources* **2005**, *141*, 129.
[39] B. T. Hang, I. Watanabe, T. Doi, S. Okada, J.-I. Yamaki, *J. Power Sources* **2006**, *161*, 1281.
[40] M. V. Reddy, G. V. Subba Rao, B. V. R. Chowdari, *Electrochim. Acta* **2005**, *50*, 375.